



This is a repository copy of *Critical Design Criterion for Achieving Zero Voltage Switching in Inductorless Half-Bridge-Driven Piezoelectric-Transformer-Based Power Supplies*.

White Rose Research Online URL for this paper:
<http://eprints.whiterose.ac.uk/90488/>

Version: Accepted Version

Article:

Foster, M.P., Davidson, J.N., Horsley, E.L. et al. (1 more author) (2015) Critical Design Criterion for Achieving Zero Voltage Switching in Inductorless Half-Bridge-Driven Piezoelectric-Transformer-Based Power Supplies. IEEE Transactions on Power Electronics. ISSN 1941-0107

<https://doi.org/10.1109/TPEL.2015.2481706>

Reuse

Unless indicated otherwise, fulltext items are protected by copyright with all rights reserved. The copyright exception in section 29 of the Copyright, Designs and Patents Act 1988 allows the making of a single copy solely for the purpose of non-commercial research or private study within the limits of fair dealing. The publisher or other rights-holder may allow further reproduction and re-use of this version - refer to the White Rose Research Online record for this item. Where records identify the publisher as the copyright holder, users can verify any specific terms of use on the publisher's website.

Takedown

If you consider content in White Rose Research Online to be in breach of UK law, please notify us by emailing eprints@whiterose.ac.uk including the URL of the record and the reason for the withdrawal request.



eprints@whiterose.ac.uk
<https://eprints.whiterose.ac.uk/>

Critical Design Criterion for Achieving Zero Voltage Switching in Inductor-Less Half-Bridge Driven Piezoelectric Transformer Based Power Supplies

Martin P. Foster, Jonathan N. Davidson, Edward L. Horsley and David A. Stone

Abstract—A methodology for predicting the ability of inductor-less driven piezoelectric transformer (PT) based power supplies to achieve zero voltage switching (ZVS) is presented. A describing function approach is used to derive an equivalent circuit model of the PT operating in the vicinity of ZVS and the subsequent application of the model provides a quantitative measure of a PT's ability to achieve ZVS when driven by an inductor-less half-bridge inverter. Through detailed analysis of the analytical model, the limitations of the inductor-less half-bridge driven PT are exposed from which guidelines for designing both the PT and inverter are derived.

Index Terms—Power conversion, Piezoelectric devices, Resonant inverters, Zero voltage switching, Design optimization

I. INTRODUCTION

RECENTLY there has been renewed interest in piezoelectric transformers (PTs) for use in power electronic applications afforded as a consequence of the advancements in materials science and the technological developments in microelectronics, allowing these devices to be deployed in existing and new applications. PTs offer many potential advantages over magnetic transformers including high-power density ($>40\text{Wcm}^{-1}$ [1]), low EMI, reduced weight, high galvanic isolation and improved efficiency [2] and for some power supply applications, they can be utilised to completely replace the magnetic transformer and inductor components. Thus, PTs are already found employed in backlighting power supplies for laptop computers, PDAs and LCD TVs [3], fluorescent and LED lighting [4-6], mobile phone battery chargers [7] and ionization and plasma generators [8].

For PTs, high efficiency is achieved when they are operated close to their primary resonant frequency where, typically, the PT is driven by a push-pull, a class-E or a half-bridge inverter [1]. The inverter switching device timings are carefully chosen to enable soft-switching to maximise overall power conversion efficiency. Owing to their relatively large input

capacitance, an additional series inductor is often used to guarantee zero-voltage-switching (ZVS) of the half-bridge; however, this has the unfortunate drawback of decreasing power density and increasing weight and cost [9]. Inductor-less half-bridge inverter driven PTs are operated without the additional series inductor so the PT and the control circuit has to be carefully selected to ensure that sufficient current is flowing in the circuit to charge the PT input capacitance (C_{in}) to the DC input voltage level (V_{in}) during the MOSFET dead-time period (t_{in}) [4, 10]. If the resonant current is of insufficient amplitude, or the dead-time period is too small, the input capacitance voltage (v_{Cin}) will not reach V_{in} before the MOSFET is turned on and switching losses will be incurred.

To guarantee ZVS, the designer has to examine the circuit under all anticipated operating conditions to determine if sufficient charge can be accrued on C_{in} during t_{in} . Resonant converters suffer from similar issues; however, the dead-time interval is usually small relative to the switching period T due to the large circulating currents involved, permitting the derivation of simplified expressions to aid design such as those provided in [11]. For PTs, the situation is not as straightforward owing to the large input capacitance and limited availability of resonant current, thus the required dead-time interval can be a significant proportion of the switching period and so the usual approximation of assuming a constant current value during the dead-time is no longer valid.

Several authors have derived models of varying accuracy to predict behaviour during the dead-time interval. In [12], the model proposed permits estimation of the ZVS ability of an inductor-less PT inverter; however, it provides overly conservative estimates owing to the waveform shape assumption made for v_{Cin} and its phase relationship to the resonant current and its application is limited since it does not accept the dead-time interval as a parameter.

A hybrid method is described in [13] where a piecewise linear state-variable model is used to determine the operating characteristics of a PT-based DC-DC converter. The model employs the fundamental mode approximation (FMA) method to represent the non-linear action of the rectifier and load using an equivalent resistor. A parallel-to-series impedance transformation is also used to reduce the model order. The duty-frequency relationship required to maintain operation with the ZVS region is found using numerical methods. Although this method appears to provide good accuracy, the

M.P. Foster, J.N. Davidson and D.A. Stone are with the Department of Electronic and Electrical Engineering, The University of Sheffield, Sir Frederick Mappin Building, Mappin Street, SHEFFIELD S1 3JD, UK (e-mail: M.P.Foster@sheffield.ac.uk Jonathan.Davidson@sheffield.ac.uk; D.A.Stone@sheffield.ac.uk).

E. L. Horsley was formerly with the University of Sheffield, Sheffield S1 3JD, U. K. He is currently with Siemens Wind Power, Keele, U. K. (e-mail: Edward.Horsley@siemens.com).

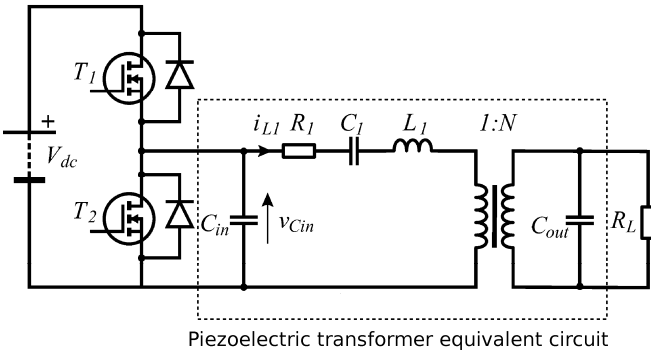


Fig. 1. Inductor-less piezoelectric transformer based power supply

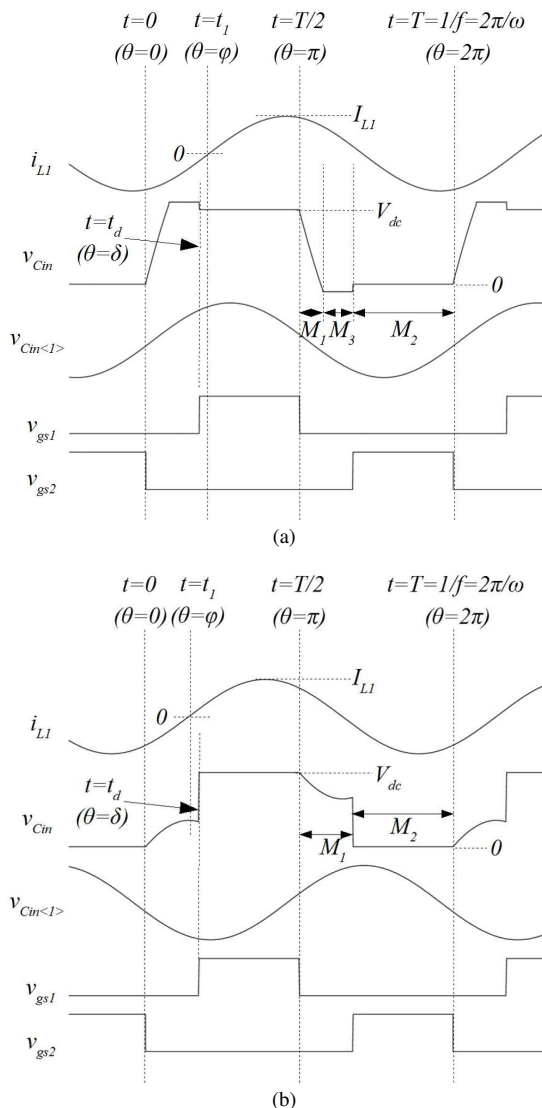


Fig. 2. Typical Mason equivalent circuit component waveforms. (a) ZVS achieved and (b) ZVS not achieved

absence of both a design example and normalised parameter analysis makes it difficult for the reader to implement.

Both [14,15] also employ a form of cyclic-mode analysis to predict the circuit waveforms, and as such provide predictions with improved accuracy since no assumptions are made

regarding the waveform shapes of the voltages and currents. These methods, however, provide only a numerical solution complicating analysis. An alternative approach is taken in [16] where the ZVS ability of a generic PT is assessed through a parametric sweep of the Mason equivalent circuit parameters and curve fitting provides a simple equation representing the ZVS ability of a PT as a function of its input and output capacitance ratio. Although good correlation is shown by this method, the relative accuracy of its predictions are questionable since it relies on a specific PT characterisation to generate the parametric sweep.

In this paper, a new model is derived to predict ZVS behaviour of an inductor-less drive PT based on a describing function approximation of v_{Cin} . Unlike the techniques mentioned previously, the methodology presented here provides an analytical model of the ZVS which can provide greater understanding of the underlying mechanisms involved. Assuming the PT is constructed from high Q -factor material, a sinusoidal current can be seen to flow in the Mason equivalent circuit creating a cosinusoidal shape voltage across C_{in} during the dead-time intervals. Since an expression for v_{Cin} is derived purely in terms of the resonant current, the final model is made independent of PT material parameters and is only characterised by the input-output capacitance ratio (C_n), dead-time (t_{in}), a load factor (M) and efficiency (η). The accuracy of the proposed model is verified against published models and experimental measurements. A critical design condition in the form of an inequality is derived to allow one to design both the PT and inverter such that ZVS can be guaranteed over the anticipated operating range.

The remaining sections of the paper are as follows: Section II describes the operation of an inductor-less half-bridge inverter driven PT and the PT equivalent circuit model. In Section III, the describing function based model for ZVS is derived. The proposed model is validated in Section IV using both experimental and simulation methods. In Section V, a detailed analysis of the ZVS abilities of PTs is provided. Section VI summarises the major findings of the work and provides design guidelines for both the PT and half-bridge inverter.

II. OPERATION OF INDUCTOR-LESS HALF-BRIDGE DRIVEN PT BASED POWER SUPPLIES

In general, it is known that a PT possesses a high Q -factor band-pass filter characteristic when operated close to its primary resonant mode, and its behaviour can be described by the Mason equivalent circuit model depicted in Fig. 1 [17]. The input capacitance (C_{in}) and output capacitance (C_{out}) correspond to the input and output terminal electrode capacitances; L_1 , C_1 and N model the acoustic mechanical resonant phenomenon; and R_1 represents the effects of mechanical damping and other losses. The half-bridge MOSFETs T_1 and T_2 are operated in anti-phase at a specific frequency. To prevent the occurrence of a shoot-through event (i.e. the simultaneous conduction of T_1 and T_2) and to achieve ZVS, there must be a sufficient dead-time interval between the gate signals of the MOSFETs: that is, high-side MOSFET (T_1) must turn off before the low-side MOSFET (T_2) turns on, and vice versa.

During a single half-cycle, the circuit shown in Fig. 1 can exist in one of only three possible circuit configurations or modes:

- M1: Both MOSFETs T_1 and T_2 are off and v_{Cin} is being charged by i_{L1} . v_{Cin} is heading towards V_{in} (or being discharged towards 0V).
- M2: MOSFET T_1 (or T_2) is on and v_{Cin} is clamped to V_{in} (or to 0V).
- M3: v_{Cin} has exceeded V_{in} (or fallen below 0V) and turned-on the anti-parallel diode of T_1 (or T_2) such that $v_{Cin}=V_{in}+V_{in1}$ (or $v_{Cin}=-V_{in2}$) where V_{inx} is the forward voltage drop of the anti-parallel diode of MOSFET T_x .

During a typical first half-cycle (T_2 turn off followed by T_1 turn on) the mode (circuit configuration) sequences M1→M2 or M1→M3→M2 are typically observed. For the purposes of analysing ZVS, only the mode sequence M1→M2 (Fig. 2b) needs to be considered since, if $v_{Cin}(t_1) \geq V_{in}$, the ZVS condition can be achieved. This assumption simplifies the following analysis by reducing the number of piecewise descriptions required for v_{Cin} and the associated unknown mode time duration. By way of example, Fig. 2 illustrates the key Mason equivalent circuit component waveforms for ZVS operation and non-ZVS operation where i_{L1} , v_{Cin} and $v_{Cin<1>}$ are the resonant current, input capacitance voltage and its fundamental component respectively and v_{gs1} and v_{gs2} are the gate signals for T_1 & T_2 respectively. The time intervals associated with the mode sequence are also shown Fig. 2 (the corresponding angles are shown in brackets). $t_{in}(\delta)$, $t_1(\phi)$ and $T(2\pi)$ are dead-time, resonant current time (phase) delay and switching period respectively. In Fig. 2a, ZVS is clearly achievable and the mode sequence here is M1→M3→M2. Under closer inspection it can be seen that the charge transferred during the dead-time interval $0 \leq t < t_d$ (or $0 \leq \theta < \delta$) exceeds that required to charge C_{in} to V_{in} and so the anti-parallel diode of T_1 conducts until T_1 is turned on at $t=t_{in}$. Since MOSFETs exhibit bi-directional current flow, negative current flows through T_1 during the interval $t_d \leq t < t_1$ (or $\delta \leq \theta < \phi$). In contrast, Fig. 2b shows typical waveforms when ZVS is not achieved. Here, v_{Cin} does not reach V_{in} during the dead-time interval $\theta = \delta$ and energy is dissipated in T_1 owing to the near instantaneous step-change in v_{Cin} that occurs as T_1 turns on. For the purposes of the analysis presented here, the dead-time interval is assumed to be optimal when $v_{Cin}(t_1) \geq V_{in}$ and thus ZVS has been achieved.

III. DERIVATION OF ZVS MODEL

In the analysis that follows, a mathematical model is developed to quantify the ability of an inductor-less driven PT to achieve ZVS. Owing to the complexities of the ZVS process, the model is derived in three stages allowing unknown quantities to be systematically eliminated resulting in an analytical solution. In Stage I an expression for the voltage at the end of the dead-time interval is obtained. This provides the ZVS metric employed by the analysis presented later in the paper. In Stage II an expression relating the magnitude of the resonant current (I_{L1}) to input voltage (V_{dc}) is obtained by equating the input energy of the circuit to the sum of the output energy, energy loss in R_1 and the energy transfer

to-and-from C_{in} during the dead-time intervals. Finally, in Stage III a non-linear expression for the current phase angle ϕ is obtained by equating the equivalent impedance of the PT (from a signal perspective) to its actual impedance as determined by the circuit components. The primary assumption employed in the analysis is that resonant current is sinusoidal which is generally the case for PTs constructed using high Q -factor materials. The analysis provides a generic model of the ZVS process which is applicable to any PT that can be described using the Mason equivalent circuit. Euler's form representation is used throughout this paper to simplify the presentation of the derivations.

A. Stage I – ZVS metric

Referring to Fig. 2, the resonant circuit current i_{L1} is defined as,

$$i_{L1}(t) = I_{L1} \sin(\omega(t + t_1))$$

or

$$i_{L1}(\theta) = I_{L1} \sin(\theta + \phi) = I_{L1} \frac{e^{j\theta} e^{j\phi} - e^{-j\theta} e^{-j\phi}}{2j} \quad (1)$$

where I_{L1} is the amplitude, $\omega = 2\pi f$ is the angular switching frequency, t_1 is the time delay and ϕ is the phase angle.

Assuming 2 modes are sufficient to describe a half-cycle (Fig. 2b), the PT input voltage (v_{Cin}) can be decomposed into four piecewise sections. When the MOSFETs are active, v_{Cin} is clamped to V_{dc} or 0V. During the dead-time intervals, the resonant current circulates through the PT's input capacitance producing a cosinusoidal shape voltage. The general form of this voltage can be found by evaluating the following integral,

$$v_{Cin}(\theta) = \frac{1}{\omega C_{in}} \int -i_{L1}(\theta) d\theta + V \quad (2)$$

where V is the constant of integration and its value is found by determining the capacitor voltage at the start of the associated operating mode, i.e. $v_{Cin}(\theta = 0) = 0$.

During the first interval, $0 < \theta \leq \delta$, the input capacitor voltage v_{Cin1} is given by,

$$v_{Cin1}(\theta) = \frac{1}{\omega C_{in}} \int_0^\delta -i_{L1} d\theta + V_1 = \frac{I_{L1}}{\omega C_{in}} \cos(\theta + \phi) + V_1 \quad (3)$$

The constant of integration, V_1 , is found by evaluating $v_{Cin}(\theta = 0) = 0$,

$$V_1 = \frac{-I_{L1}}{\omega C_{in}} \cos(\phi) \quad (4)$$

Thus,

$$v_{Cin1}(\theta) = \frac{I_{L1}}{\omega C_{in}} [\cos(\theta + \phi) - \cos(\phi)] \quad (5)$$

During the third interval, $\pi < \theta \leq \pi + \delta$, the input capacitor voltage is given by,

$$\int_{\pi}^{\pi+\delta} -i_{L1} d\theta + V_3 = \frac{I_{L1}}{\omega C_{in}} [\cos(\theta + \phi) + \cos(\phi)] + V_{dc} \quad (6)$$

where the constant of integration is found by evaluating $v_{Cin}(\pi) = V_{dc}$.

During the interval $0 \leq \theta < \delta$, v_{Cin} charges from 0 to $K_{zvs} \times V_{dc}$ using the resonant current, where K_{zvs} is a normalising parameter relating the actual change in v_{Cin} relative to the DC input voltage and for $K_{zvs} \geq 1$ ZVS is achieved. By applying Euler's form to (5) the ZVS metric is given by,

$$K_{zvs} = \frac{I_{L1}}{V_{dc} \omega C_{in}} \left[\frac{e^{j(\delta+\phi)} + e^{-j(\delta+\phi)}}{2} - \frac{e^{j\phi} + e^{-j\phi}}{2} \right] \quad (7)$$

B. Stage II – Removal of I_{L1} dependence

In this stage an expression for V_{dc} in terms of I_{L1} will be obtained and substituted into (7) to provide a ZVS metric that is dependent only on the PT equivalent circuit parameters and load. This expression is obtained by considering the energy supplied to the circuit by V_{dc} , the energy dissipated in both the load (R_L) and the PT equivalent circuit loss resistor (R_1) and the change in energy experienced by C_{in} during one complete cycle. Energy is transferred to the PT only during the interval $\delta \leq \theta < \pi$. Evaluating the energy integral over this period gives the input energy,

$$E_{in} = \frac{1}{\omega} \int_{\delta}^{\pi} V_{dc} i_{L1}(\theta) d\theta = \frac{V_{dc} I_{L1}}{2\omega} [e^{j\phi}(1 + e^{j\delta}) + e^{-j\phi}(1 + e^{-j\delta})] \quad (8)$$

Since the resonant current i_{L1} circulates through C_{out} and R_L for the duration of the cycle, the energy dissipated in the output is given by,

$$E_{out} = \frac{1}{\omega} \int_0^{2\pi} \frac{V_{out}^2}{R_L} d\theta = \frac{I_{L1}^2 R_L \pi}{\omega N^2 (1 + \omega^2 C_{out}^2 R_L^2)} \quad (9)$$

where $V_{out} = i_{L1}(\theta) / (N \sqrt{1/R_L^2 + \omega^2 C_{out}^2})$.

A similar expression for the energy dissipated in R_1 is obtained,

$$E_{R1} = \frac{I_{L1}^2 R_1 \pi}{\omega} \quad (10)$$

Now consider the energy used to charge and discharge the input capacitance during a single cycle. The change in energy stored in C_{in} from the beginning to the end of the dead-time period is given by,

$$E_1 = \frac{C_{in} v_{Cin}(\delta)^2}{2} = \frac{I_{L1}^2}{8\omega^2 C_{in}} [e^{j(\delta+\phi)} + e^{-j(\delta+\phi)} - (e^{j\phi} + e^{-j\phi})]^2 \quad (11)$$

During interval 3 the change in energy stored in C_{in} is given by (12). Combining the two energies provides the total change in stored energy experienced by C_{in} produces (13).

From the conservation of energy principle, the input energy is equal to the energy dissipated in the load + energy stored + losses. This leads to two possible methods for determining the input energy: one based on losses (equation (14)) and the other based on efficiency, η (equation (15)),

$$E_{in} = E_{out} + E_{Cin} + E_{R1} \quad (14)$$

$$E_{in} = \frac{E_{out} + E_{Cin}}{\eta} \quad (15)$$

For the purposes of mathematical analysis, these can be combined to a single equation by introducing a selecting parameter, α , as shown in (16). Setting $\alpha = 1$ produces (14) and results in a loss-based study, whereas setting $\alpha = 0$ produces (15) and results in an efficiency-based study.

$$E_2 = \frac{C_{in} v_{Cin}(\pi + \delta)^2}{2} - \frac{C_{in} v_{Cin}(\pi)^2}{2} = \frac{I_{L1}^2}{8\omega^2 C_{in}} [e^{j\phi}(1 - e^{j\delta}) + e^{-j\phi}(1 - e^{-j\delta})]^2 + \frac{V_{dc} I_{L1}}{2\omega} [e^{j\phi}(1 - e^{j\delta}) + e^{-j\phi}(1 - e^{-j\delta})] \quad (12)$$

$$E_{Cin} = E_1 + E_2 = \frac{I_{L1}^2}{4\omega^2 C_{in}} \{e^{j2\phi} [e^{j2\delta} - 2e^{j\delta} + 1] + e^{-j2\phi} [e^{-j2\delta} - 2e^{-j\delta} + 1] - 2(e^{j\delta} + e^{-j\delta} - 2)\} + \frac{V_{dc} I_{L1}}{2\omega} [e^{j\phi}(1 - e^{j\delta}) + e^{-j\phi}(1 - e^{-j\delta})] \quad (13)$$

$$V_{dc} = \frac{2I_{L1}}{\left(e^{j\phi}(1 + e^{j\delta}) + e^{-j\phi}(1 + e^{-j\delta}) - \frac{1}{\eta'} [e^{j\phi}(1 - e^{j\delta}) + e^{-j\phi}(1 - e^{-j\delta})] \right)} \times \left[\alpha R_1 \pi + \frac{R_L \pi}{\eta' N^2 (1 + \omega^2 C_{out}^2 R_L^2)} + \frac{1}{4\eta' \omega C_{in}} \{e^{j2\phi} [e^{j2\delta} - 2e^{j\delta} + 1] + e^{-j2\phi} [e^{-j2\delta} - 2e^{-j\delta} + 1] - 2(e^{j\delta} + e^{-j\delta} - 2)\} \right] \quad (17)$$

$$E_{in} = \frac{E_{out} + E_{Cin}}{\eta'} + \alpha E_{R1} \quad (16)$$

where $\eta' = (1 - \alpha)\eta + \alpha$ (i.e. $\eta' = 1$ for a loss-based study and $\eta' = \eta$ for an efficiency-based study). Substituting equations (8)-(10) and (13) into (16) and rearranging provides an expression (17) for the input voltage in terms of the resonant current and the equivalent circuit components.

Substituting (17) into (7) and introducing the normalising parameters given in (19) for series resonant frequency (ω_0), normalised operating frequency (ω_n), quality factor (Q), input-to-output capacitance ratio (C_n), resonant-to-output capacitance ratio (A) and the normalised load factor (M), provides an analytical expression (18) for the ZVS metric.

C. Stage III – Determine the resonant current phase angle ϕ

A value for the resonant current phase angle, ϕ , is found through the solution of a non-linear equation that is obtained by equating the component-based input impedance of the PT equivalent circuit to the signal-based equivalent impedance. The signal-based impedance is found through the application of Ohm's law by dividing the describing function approximation of the PT's input voltage ($v_{Cin<1>}$) by the fundamental of the resonant current using a technique similar to those presented in [18,19]. The describing function, $v_{Cin<1>}$, is found by extracting the fundamental component from the Fourier series of v_{Cin} . To simplify this process, a modified expression for v_{Cin} is derived by subtracting DC offset ($V_{dc}/2$) to allow the Fourier transform to be evaluated over a half-cycle. From inspection of Fig. 2, (5) and (6), a piecewise description for the modified input capacitor voltage is given by,

$$v_{Cin}(\theta) = \begin{cases} \frac{I_{L1}}{\omega C_{in}} \left[\frac{e^{j(\theta+\phi)} + e^{-j(\theta+\phi)}}{2} - \frac{e^{j\phi} + e^{-j\phi}}{2} \right] - \frac{V_{dc}}{2} & 0 \leq \theta < \delta \\ \frac{V_{dc}}{2} & \delta \leq \theta < \pi \\ \frac{I_{L1}}{\omega C_{in}} \left[\frac{e^{j(\theta+\phi)} + e^{-j(\theta+\phi)}}{2} + \frac{e^{j\phi} + e^{-j\phi}}{2} \right] + \frac{V_{dc}}{2} & \pi \leq \theta < \pi + \delta \\ \frac{-V_{dc}}{2} & \pi + \delta \leq \theta < 2\pi \end{cases} \quad (20)$$

Using the same definition for the complex Fourier series as employed in [19], only the first half-cycle need to be considered. Thus,

$$v_{Cin<1>} = \frac{2}{\pi} \int_0^\pi v_{Cin}(\theta) e^{-j\theta} d\theta \quad (21)$$

Evaluating $v_{Cin<1>}$ over the first interval, $0 \leq \theta < \delta$, leads to,

$$v_{Cin<1>a} = \frac{I_{L1}}{\pi \omega C_{in}} \left[e^{j\phi} \delta + \frac{e^{-j\phi}}{2j} (1 - e^{-j2\delta}) + \frac{e^{j\phi} + e^{-j\phi}}{j} (e^{-j\delta} - 1) \right] + \frac{V_{dc}}{j\pi} [e^{-j\delta} - 1] \quad (22)$$

Similarly, application over the second interval, $\delta \leq \theta < \pi$, leads to,

$$v_{Cin<1>b} = \frac{V_{dc}}{\pi j} (e^{-j\delta} + 1) \quad (23)$$

Combining (22) and (23), substituting (17) and employing the normalising terms (19) provides (24). The signal-based equivalent input impedance is then found using Ohm's law,

$$K_{zvs} = \frac{e^{j\phi} \gamma_3 + e^{-j\phi} \gamma_4}{4\omega_n C_n} \times \frac{e^{j\phi} \gamma_1 + e^{-j\phi} \gamma_2 + \frac{1}{\eta'} [e^{j\phi} \gamma_3 + e^{-j\phi} \gamma_4]}{\left(\frac{\alpha\pi}{AQ} + \frac{\pi M}{\eta' (1 + \omega_n^2 M^2)} + \frac{1}{4\eta' \omega_n C_n} \{ e^{j2\phi} \gamma_3^2 + e^{-j2\phi} \gamma_4^2 - 2(e^{j\delta} + e^{-j\delta} - 2) \} \right)} \quad (18)$$

where

$$\gamma_1 = e^{j\delta} + 1, \gamma_2 = e^{-j\delta} + 1, \gamma_3 = e^{j\delta} - 1, \gamma_4 = e^{-j\delta} - 1,$$

$$\omega_0 = \frac{1}{\sqrt{L_1 C_1}}, \omega_n = \frac{\omega}{\omega_0}, Q = \frac{\omega_0 L_1}{R_1} = \frac{1}{\omega_0 C_1 R_1}, C_n = \frac{C_{in}}{N^2 C_{out}}, A = \frac{C_1}{N^2 C_{out}}, M = R_L \omega_0 C_{out} \quad (19)$$

$$v_{Cin<1>} = \frac{I_{L1}}{\pi \omega_0 N^2 C_{out}} \left[\frac{1}{\omega_n C_n} \left[e^{j\phi} \delta + \frac{e^{-j\phi}}{2j} (1 - e^{-j2\delta}) + \frac{e^{j\phi} + e^{-j\phi}}{j} \gamma_4 \right] + \frac{4}{j} e^{-j\delta} \frac{\left(\frac{\alpha\pi}{AQ} + \frac{\pi M}{\eta' (1 + \omega_n^2 M^2)} + \frac{1}{4\eta' \omega_n C_n} \{ e^{j2\phi} \gamma_3^2 + e^{-j2\phi} \gamma_4^2 - 2(e^{j\delta} + e^{-j\delta} - 2) \} \right)}{e^{j\phi} \gamma_1 + e^{-j\phi} \gamma_2 + \frac{1}{\eta'} [e^{j\phi} \gamma_3 + e^{-j\phi} \gamma_4]} \right] \quad (24)$$

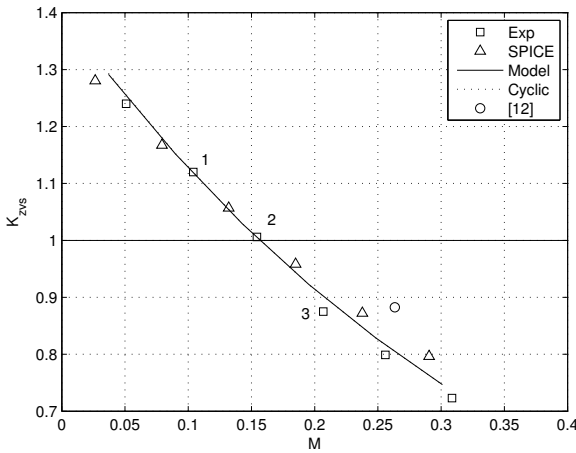


Fig. 1. ZVS performance of Transoner T1-22 PT as a function of load factor ($\omega_n = 1.027$)

$$Z_{in} = \frac{v_{Cin<1>}}{I_{L1}} j e^{-j\phi} \quad (25)$$

The component-based input impedance is the impedance looking into the PT input terminals ignoring C_{in} . Employing basic circuit analysis and after applying the normalising parameters it is given by,

$$Z_{in} = \frac{1}{N^2 \omega_0 C_{out}} \left[\frac{j}{A} \left(\omega_n - \frac{1}{\omega_n} \right) + \frac{\alpha}{AQ} + \frac{M}{1 + j\omega_n M} \right] \quad (26)$$

Equating (25) and (26) provides an equation (27) that must be solved using numerical methods to determine the current phase angle, ϕ .

IV. VALIDATION OF THE PROPOSED MODEL

For a given PT, C_n is fixed and so (18) can be used to provide a quantitative assessment of whether a PT is capable of achieving ZVS when driven by an inductor-less inverter. By way of example, Fig. 3 shows the ZVS metric (K_{zvs}) as a function of the load factor M for a Transoner® T1-22 radial mode PT operating at a frequency of 122.6kHz with a dead-time of 2.2 μ s. The Mason equivalent circuit parameters of the PT measured when connected to a matched load are $C_{in} = 1.96$ nF, $C_{out} = 1.41$ nF, $L_1 = 10.1$ mH, $C_1 = 176$ pF, $R_1 = 5.64$ Ω (this is a loss-based analysis so $\alpha = 1$), and $N = 0.915$.

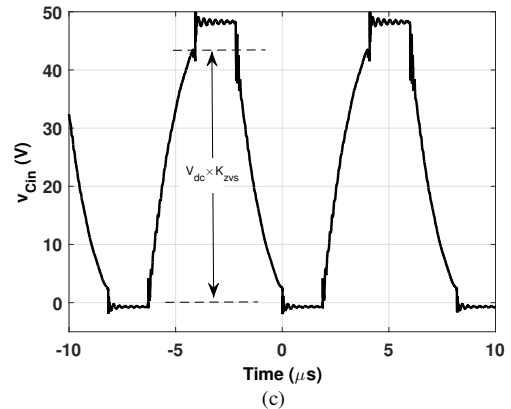
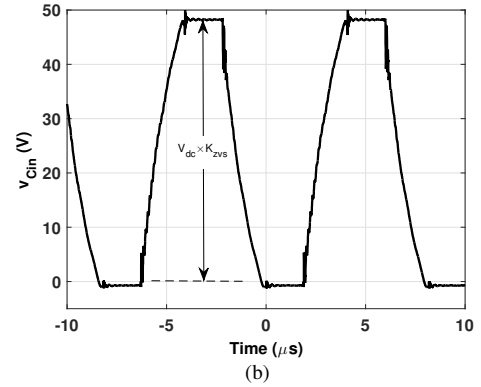
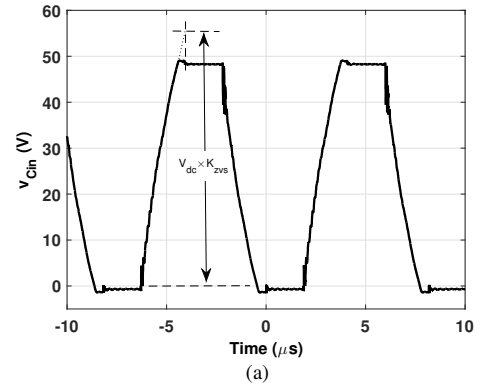


Fig. 4. Experimental measured v_{Cin} waveforms. (a) $K_{zvs} > 1$, (b) $K_{zvs} \sim 1$, (c) $K_{zvs} < 1$ (Fig. 3 points 1-3 respectively).

Since IRF510 MOSFETs were used in a half-bridge inverter with $V_{dc} = 48$ V, the input capacitance of the PT is modified by their parasitic output capacitance (taken to be ~ 260 pF) and so

$$0 = \frac{e^{-j\phi}}{\pi} \left[\frac{j}{\omega_n C_n} \left[e^{j\phi} \delta + \frac{e^{-j\phi}}{2j} (1 - e^{-j2\delta}) + \frac{e^{j\phi} + e^{-j\phi}}{j} (e^{-j\delta} - 1) \right] + 4e^{-j\delta} \frac{\left(\frac{\alpha\pi}{AQ} + \frac{\pi M}{\eta'(1 + \omega_n^2 M^2)} + \frac{1}{4\eta' \omega_n C_n} \{ e^{j2\phi} \gamma_3^2 + e^{-j2\phi} \gamma_4^2 - 2(e^{j\delta} + e^{-j\delta} - 2) \} \right)}{e^{j\phi} \gamma_1 + e^{-j\phi} \gamma_2 + \frac{1}{\eta'} [e^{j\phi} \gamma_3 + e^{-j\phi} \gamma_4]} \right] - \left[\frac{j}{A} \left(\omega_n - \frac{1}{\omega_n} \right) + \frac{\alpha}{AQ} + \frac{M}{1 + j\omega_n M} \right]$$

a value of 2.21 nF was used for C_{in} . As can be seen, the proposed model correlates well with experimental measurements and SPICE, and for this particular PT, ZVS is achievable for all load resistor values below $\sim 140 \Omega$ when operated with the frequency and dead-time interval values specified. The results are almost indistinguishable from those predicted using the cyclic-mode model described in [15] (as a result, the cyclic curve is entirely obscured by the curve predicted by the proposed model). For completeness, comparison is also made using the method presented in [12], indicated by the circle marker. Only a single point is compared because this model cannot provide predictions with the dead-time interval as a model parameter. As can be seen there is a discrepancy between predictions using [12] and both the proposed model and the experimental results. This inaccuracy is a consequence of the approximations and assumptions made during the derivation in [12].

Fig 4 shows the experimental measurements of v_{Cin} for points labelled 1-3 in Fig 3, illustrating the different waveform shapes of v_{Cin} typically encountered under ZVS and non-ZVS operation and shows how K_{zvs} is determined. It can be seen from (18) that K_{zvs} also depends on the dead-time interval. For a given load factor and operating frequency, there is an ideal dead-time (the value of which is discussed in section V). For the results depicted in Figs. 3 and 4, the dead-time value was selected to provide maximum K_{zvs} . For certain operating conditions ZVS is unachievable ($K_{zvs} < 1$). This is the case for Fig. 4(c) where specifically there is no value for the dead-time that will result in ZVS.

The 3D plot depicted in Fig. 5 highlights the dependence of K_{zvs} on both the operating frequency and the load for the same fixed dead-time interval employed to generate Fig. 3. The actual parameter range covered by Fig. 3 is indicated by a solid black line. The T1-22 PT exhibits two distinct regions where inductor-less ZVS can be achieved (indicated by the shaded area) with one at very high loads and the other at very low loads, and so in order to maintain ZVS, and hence maximise efficiency, the regulator would need to simultaneously control the frequency and the dead-time which is difficult to achieve when there are two disconnected regions. The difficulty of the problem is highlighted by [20] which shows the complex circuitry and control design necessary to regulate output voltage through simultaneous frequency and dead time control. It should be noted that the T1-22 PT cannot achieve inductor-less ZVS for the matched load ($M = 1$), a specific operating condition one would usually associate with maximum efficiency [17].

Figure 6 presents the ZVS profile for the T1-PP0361 radial-mode transformer, which has been designed to operate with lower impedance loads than the T1-22 PT, and clearly shows that ZVS is achievable over a wider range of operating conditions. The T1-PP0361 PT has the following equivalent circuit component values measured with the PT connected to a matched load: $C_{in} = 4.93$ nF, $C_{out} = 2.7$ nF, $L_1 = 4.48$ mH, $C_1 = 891$ pF, $R_1 = 4.34 \Omega$ ($\alpha = \eta' = 1$), $N = 2.21$ and $t_d = 3.75 \mu s$. To achieve ZVS the input capacitance needs to accumulate sufficient charge during the dead-time interval for its voltage to reach V_{dc} and thus the circulating current needs to be of sufficient amplitude and phase. Since the T1-22 PT has a relatively large input capacitance, significant charge is

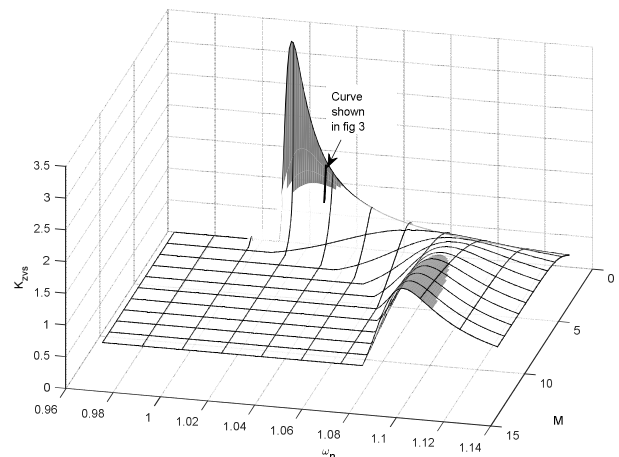


Fig 5. ZVS operating regions of the T1-22 PT (shaded regions are where $K_{zvs} \geq 1$)

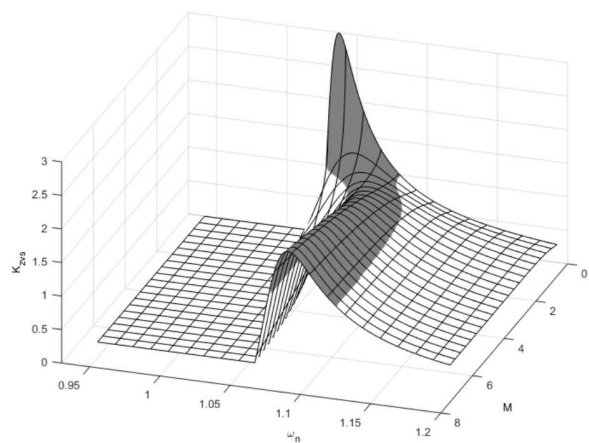


Fig. 6. ZVS operating characteristic for the T1-PP0361 PT (shaded region is where $K_{zvs} \geq 1$)

required to charge v_{Cin} to V_{dc} and this is only available for specific operating conditions (i.e. the regions of light and heavy loading regions shown in Fig. 5). By comparison, the input capacitance of the T1-PP0361 PT is relatively small and inductor-less ZVS can be easily achieved over a wider range of operating conditions. Thus, Figs. 5 and 6 clearly demonstrate the importance of considering C_{in} and the load range when designing an inductor-less driven PT based circuit.

To further validate the accuracy of the proposed model, a comparison was made with the cyclic-mode model described in [14]. Figure 7a and 7b show the percentage error (log-scale) in K_{zvs} between the proposed and the cyclic-mode model for the T1-22 and T1-PP0361 PTs respectively demonstrating the proposed model correlates well. As can be seen the actual percentage error is very small (average $< 1\%$).

V. ANALYSIS OF INDUCTOR-LESS DRIVEN PTs

Referring to the shaded regions in Figs. 5 and 6, it can be seen there are operating conditions where inductor-less ZVS can be achieved. In this section the proposed model is used to develop a design criterion for PT and the inverter to ensure ZVS is guaranteed for all operating conditions. From (5), one

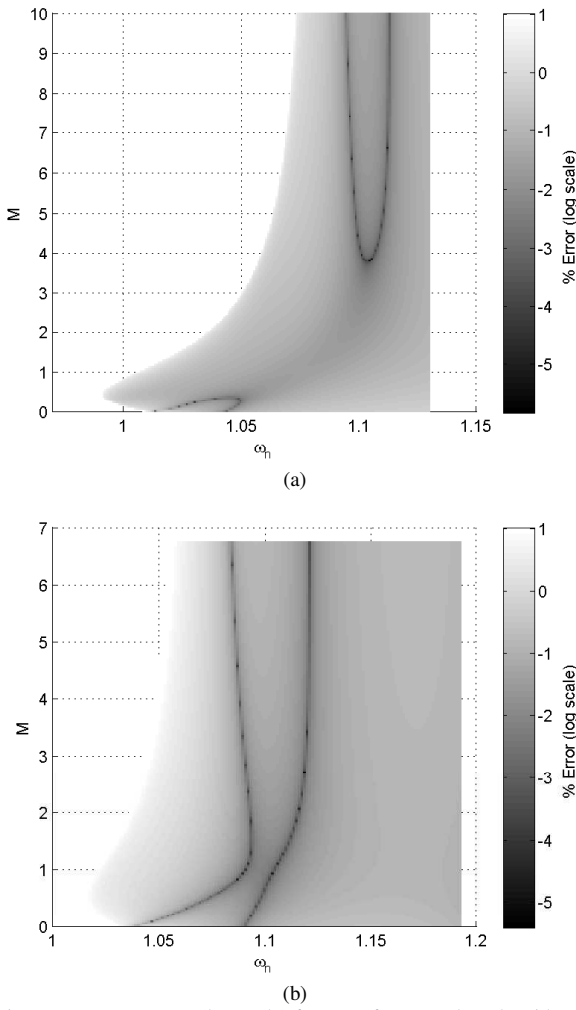


Fig. 7. Percentage error (log-scale) for K_{zvs} of proposed mode with respect to cyclic-mode. (a) T1-22 PT and (b) T1-PP0361 PT

can see that the value of input capacitor voltage at the end of the dead-time period, $v_{cin}(\delta)$, is maximised when,

$$\delta = -\phi = \frac{\pi}{2} \quad (28)$$

and to guarantee ZVS,

$$K_{zvs} \geq 1 \quad (29)$$

Therefore, the maximum input-output capacitor ratio that is guaranteed to achieve ZVS can be found by substituting $\alpha = 0$, (28) and (29) into (18), which, after some manipulations leads to,

$$C_n \leq \frac{\eta(1 + \omega_n^2)}{\pi\omega_n} \quad (30)$$

Due to their high Q -factor, PTs are usually operated at or just above the resonant frequency and so substituting $\omega_n \approx 1$ into (30) and assuming an ideal operating efficiency of 100% (practical PTs are highly efficient [21]) provides,

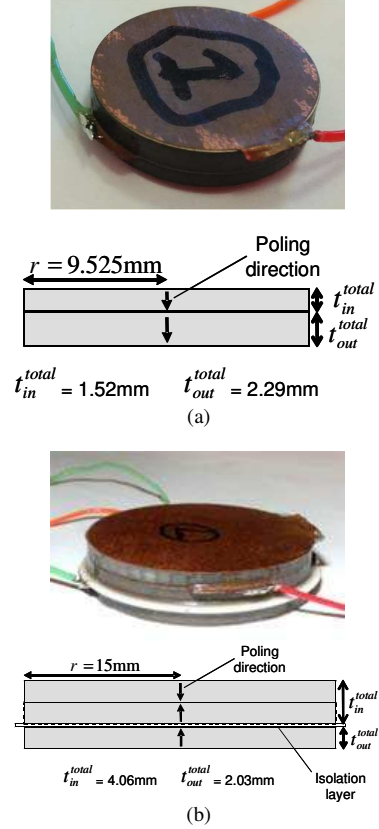


Fig. 8. Geometry of the (a) T1-22 PT and (b) T1-PP0361 PT

$$C_n \leq \frac{2}{\pi} \quad (31)$$

Finally, substituting (28), (31) and $\alpha = 0$ into (24) provides the phase relationship of the fundamental of the input capacitor voltage to be $\tan^{-1}(\pi/2) \approx 57.52^\circ$. Therefore, to ensure ZVS is achievable one must ensure the input-capacitor ratio and the dead-time angle meet the ZVS criterion below,

$$C_n \leq \frac{2}{\pi} \text{ and } \delta = \frac{\pi}{2} \quad (32)$$

These findings are very similar to those presented in [22] based on a detailed numerical analysis of the cyclic-mode model presented in [15]. It should be noted that the capacitor ratio value derived here is some 30% smaller than the value presented in [12] where $C_n \leq 32\sqrt{6}/(9\pi^2) \approx 0.72$.

Returning to the two PTs previously investigated, the physical construction for each transformer is somewhat different, Fig. 8. The T1-22 PT (Fig. 8a) has smaller radius (r) and larger input-output layer thickness ratio providing an input-output capacitance ratio of $C_n = 1.88 > 2/\pi$ (measured value incorporating MOSFET output capacitance) and therefore it can only achieve ZVS for specific operating regions. In contrast, the T1-PP0361 PT (Fig. 8b) has an input-output capacitor ratio of $C_n = 0.374 < 2/\pi$ and so ZVS is easily

achieved. Indeed, the low value of C_n provides scope for operating with reduced dead-time intervals.

VI. DISCUSSION AND GUIDELINES FOR DESIGNERS

From the analysis presented here it can be seen that ZVS of inductor-less half-bridge inverter driven PTs can be guaranteed for all load conditions if a PT's input-output capacitance ratio is $C_n \leq 2/\pi$ and if the inverter operates with a dead-time angle $\delta=90^\circ$ (assuming the PT is operated close its primary resonance and the losses are negligible). In the case where the losses are significant (i.e. $R_1 \gg 0$, $\eta < 1$) then C_n can be reduced according to (30). This capacitance ratio inequality places restrictions on the size/geometry of the input and output electrodes which must be accounted for during the PT design process if inductor-less ZVS operation is required. Thus, to guarantee success the PT designer not only has to wrestle with the physical design of the PT to ensure spurious vibration modes are suppressed and temperature rise is not excessive but also the equivalent circuit parameters are compatible with the ZVS critical design criterion. For instance, if one is designing a single layer radial-mode PT to operate with a specified load then the operating frequency, and the material properties, would dictate the PT radius which places restrictions on the size of the electrode affecting the input-output capacitance ratios [23]. Similar rules may be derived to aid the design other types of PTs including the ring type [7], disc-shape [24] and Rosen [25,26].

Output voltage, or current regulation, is a normal requirement for a practical implementation of an inductor-less PT-based power supply. Regulation can be achieved in several ways including: modulating the operating frequency [27] (and hence modulating the reactance of the resonant tank); by modulating the dead-time interval [6] (and therefore the duty cycle); or by using a burst-fire hysteresis controller when the output voltage or current is too high [28]. Where operating frequency modulation is used, the PT must be designed such that $K_{ZVS} \geq 1$ over the working range of frequencies. It can be seen in Fig. 6, for example, that ZVS is achieved for a continuous region of operating frequencies over the load range considered. Where dead-time modulation is used, the design would need to ensure that $K_{ZVS} \geq 1$ calculated from (18) and (27), is satisfied over the applicable of operating conditions. In the case of burst-fire control, the transformer operates at (or close to) resonance as described in this paper when energised, and therefore adjustment of the switch timings is not necessary.

VII. CONCLUSION

A methodology for predicting the ability of an inductor-less driven PT based inverter to achieve zero voltage switching (ZVS) has been presented. Taking a describing function approach, owing to the presence of a sinusoidal resonating current, an analytical model of the PT operating in the vicinity of ZVS has been derived to describe the shape of the input capacitor voltage during the dead-time interval and provide a quantitative measure of a PT's ability to achieve ZVS. The general conditions required to achieve ZVS have been explored and specific recommendations regarding the design of both the piezoelectric transformer and inverter control

circuit have been provided. The analysis has shown that ZVS can be guaranteed for all PTs if the design adheres to the ZVS critical design criterion presented.

REFERENCES

- [1] A. V. Carazo, "50 Years of piezoelectric transformers. Trends in the technology", in Proc. Materials Research Society Symp., 2003.
- [2] A. M. Flynn and S. R. Sanders, "Fundamental limits on energy transfer and circuit considerations for piezoelectric transformers", IEEE Trans. Power Electronics, vol. 17, pp.8-14, 2002.
- [3] Y. C. Wang, J. J. He, Y. P. Liu, J. Wu and C. K. Lee, "Theory and experiment of high voltage step-up ratio disk type piezoelectric transformer for LCD-TV", IEEE International Conference on Mechatronics 2005, pp. 284 – 287.
- [4] R. L. Lin, F. C. Lee, E. M. Baker and D. Y. Chen, "Inductor-less piezoelectric transformer electronic ballast for linear fluorescent lamp", Proc. IEEE Applied Power Electronics Conf. and Exp., 2001, vol. 2, pp. 664-669.
- [5] Song-Ling Yang ; Shih-Ming Chen ; Cheng-Che Tsai ; Cheng-Shong Hong ; Sheng-Yuan Chu, "Fabrication of high-power piezoelectric transformers using lead-free ceramics for application in electronic ballasts", IEEE Ultrasonics, Ferroelectrics and Frequency Control, vol. 60, iss. 2, pp. 408 – 413, 2013.
- [6] M. S. Røedgaard, M. Weirich and M. A. E. Andersen, "Forward Conduction Mode Controlled Piezoelectric Transformer-Based PFC LED Drive" IEEE Power Electronics, vol. 28, iss. 10, pp. 4841 – 4849, 2013.
- [7] J. Navas, T. Bove, J. A. Cobos, F. Nuno, F. and K. Brebol, "Miniaturised battery charger using piezoelectric transformers", Proc. IEEE Applied Power Electronics Conf. and Exp., 2001, vol.1, pp.492-496.
- [8] B. T. Hutsel, S. D. Kovaleski and Jae Wan Kwon, "Optimization of Piezoelectric Resonance Effect in a Piezoelectric Transformer Plasma Source", IEEE Plasma Science, vol. 41, iss. 2, pp. 305 – 311, 2013.
- [9] M. Sanz, P. Alou, R. Prieto, J. A. Cobos, and J. Uceda, "Comparison of different alternatives to drive piezoelectric transformers", Proc. IEEE Applied Power Electronics Conf. and Exp., 2002.
- [10] S. Bronstein and S. S. Ben-Yaakov, "Design considerations for achieving ZVS in a half bridge inverter that drives a piezoelectric transformer with no series inductor", in Proc. IEEE Applied Power Electronics Conf. and Exp., 2002, vol.2, pp.585-590.
- [11] B. Lu, W. Liu; Y. Liang; F. C. Lee, and J. D. Van Wyk, "Optimal design methodology for LLC resonant converter" in Proc. Applied Power Electronics Conf. and Exp., 2006, pp. 19- 23.
- [12] K. S. Meyer, M. A. E. Andersen, and F. Jensen, "Parameterized analysis of Zero Voltage Switching in resonant converters for optimal electrode layout of Piezoelectric Transformers", in Proc. IEEE Power Electronics Specialists Conf., 2008, pp.2543- 2548.
- [13] F. E. Bisogno, M. Radecker, A. Knoll, A. V. Carazo, A. Riedlhammer, G. Deboy, N. Norvez & J. M. Pacas, "Comparison of resonant topologies for step-down applications using piezoelectric transformers", IEEE Power Electronics Specialists Conf., 2004, Vol. 4, pp. 2662 – 2667.
- [14] M. P. Foster, E. L. Horsley and D. A. Stone, "Predicting the zero-voltage switching profiles of half-bridge driven inductor-less piezoelectric transformer-based inverters", IET Power Electronics vol. 5, no. 7, pp. 1068-1073, Aug. 2012
- [15] E. L. Horsley, A. V. Carazo, N. Nguyen-Quang, M. P. Foster and D. A. Stone, "Analysis of Inductorless Zero-Voltage-Switching Piezoelectric Transformer-Based Converters", IEEE Trans. Power Electronics, vol. 27, iss. 5, May 2012.
- [16] M. S. Røedgaard, T. Andersen and M. A. E. Andersen, "Empiric analysis of zero voltage switching in piezoelectric transformer based resonant converters", in Proc. IET Power Electronics, Machines and Drives Conference, 2012.
- [17] G. Ivensky, I. Zafrany, and S. S. Ben-Yaakov, "Generic operational characteristics of piezoelectric transformers", IEEE Trans. Power Electronics, vol. 17, pp. 1049-1057, 2002.
- [18] M. P. Foster, H. I. Sewell, C. M. Bingham, and D. A. Stone, "Methodologies for the design of LCC voltage-output resonant converters", IEE Proc. Electric Power Applications, vol. 153, no. 4, July 2006.

- [19] A. J. Forsyth, G. A. Ward and S. V. Mollov, "Extended fundamental frequency analysis of the LCC resonant converter", IEEE Trans. Power Electronics, vol.18, no.6, pp.1286-1292, Nov. 2003.
- [20] M. Radecker, F. Bisogno and M. Herfurth, "Control circuit for a switch unit of a clocked power supply circuit, and resonant converter", U.S. Patent 7969754 B2, June 2011
- [21] J. Erhart, P. Pulpan, R. Dolecek, P. Psota and V. Ledl, "Disc Piezoelectric Ceramic Transformers", IEEE Transactions on Ultrasonics, Ferroelectrics and Frequency Control, vol. 60, no. 8, August 2013.
- [22] E. L. Horsley, "Modelling and Analysis of Radial Mode Piezoelectric Transformers and Inductor-less Resonant Power Converters", PhD Thesis, The University of Sheffield, UK, 2011.
- [23] E. L. Horsley, A. V. Carazo, M. P. Foster & D. A. Stone; "A lumped equivalent circuit model for the radial mode piezoelectric transformer", IEEE Applied Power Electronics Conference and Exhibition 2009.
- [24] S.-L. Yang; S.-M. Chen; C.-C. Tsai; C.-S. Hong; S.-Y. Chu, "Fabrication of high-power piezoelectric transformers using lead-free ceramics for application in electronic ballasts", IEEE Ultrasonics, Ferroelectrics and Frequency Control, vol.60, no.2, pp.408,413, February 2013.
- [25] C. Nadal & F. Pigache; "Multimodal electromechanical model of piezoelectric transformers by Hamilton's principle," IEEE Ultrasonics, Ferroelectrics and Frequency Control, vol.56, no.11, pp.2530,2543, November 2009.
- [26] C. Nadal, F. Pigache and J Erhart, "Modelling of a ring rosen-type piezoelectric transformer by Hamilton's principle", IEEE Transactions on Ultrasonics, Ferroelectrics and Frequency Control, vol. 62, no. 114, April 2015.
- [27] T. Zaitso, T. Shigehisa, T. Inoue, M. Shoyama and T. Ninomiya, "Piezoelectric transformer converter with frequency control", in Proc. Telecommunications Energy Conference INTELEC 1995, Nov 1995.
- [28] J. Diaz, F. Nuno, M. J. Prieto, J. A. Martin-Romos and P. J. V. Saiz, "Closing a second feedback loop in a DC-DC converter based on a piezoelectric transformer", IEEE Transactions on Power Electronics, vol. 22, no. 6, November 2007.



Martin P. Foster received the B.Eng. degree in electronic and electrical engineering, the M.Sc. (Eng.) degree in control systems, and the Ph.D. degree for his thesis "Analysis and Design of High-order Resonant Power Converters" from the University of Sheffield, Sheffield, U.K., in 1998, 2000, and 2003, respectively.

In 2003, he became a member of academic staff at Sheffield specialising in power electronic systems and was made Senior Lecturer in 2010 and then Reader in 2014. His current research interests include the modelling and control of switching power converters, resonant power supplies, multilevel converters, battery management, piezoelectric transformers, power electronic packaging, and autonomous aerospace vehicles.



Jonathan N. Davidson received the M.Eng. degree in electronic engineering and the Ph.D. degree in thermal modelling and management from the University of Sheffield, Sheffield, U.K. in 2010 and 2015, respectively.

In 2015 he became a lecturer in multidisciplinary engineering at the University of Sheffield. His research interests include thermal modelling and management of power electronics, and the design and analysis of piezoelectric transformer-based power converters.

Dr. Davidson is a member of the Institution of Engineering and Technology.



Edward L. Horsley received the M.Eng. degree in Electronic and Electrical Engineering and the Ph.D. degree both from the University of Sheffield, Sheffield, U.K., in 2006 and 2011, respectively. He was formerly a Research Associate with the University of Sheffield. He is now with Siemens Wind Power, Keele, UK. His research interests include frequency converters, piezoelectric transformers, and resonant power converters.



David A. Stone received the B.Eng. degree in electronic engineering from the University of Sheffield, Sheffield, U.K., in 1984 and the Ph.D. degree from Liverpool University, Liverpool, U.K., in 1989.

He then returned to the University of Sheffield as a member of academic staff specialising in power electronics and machine drive systems. His current research interests are in hybrid-electric vehicles, battery management, EMC, and novel lamp ballasts for low pressure fluorescent lamps.